

# Application of Digital Image Correlation to Material Parameter Identification using LS-OPT<sup>®</sup>

Nielen Stander<sup>1</sup>, Katharina Witowski<sup>2</sup>, Christian Ilg<sup>2</sup>, Andre Haufe<sup>2</sup>, Martin Helbig<sup>2</sup>, David Koch<sup>2</sup>

<sup>1</sup>Livermore Software Technology Corporation, Livermore, CA, USA

<sup>2</sup>DYNAmore GmbH, Stuttgart, Germany

## 1 Introduction

The goal of material parameter identification is to characterize the constitutive behavior using experimental results in combination with structural modeling of the test samples. Although rather well established, it is a complex subject which may involve material nonlinearity [3,9], hysteretic behavior (loading and unloading) [9], strain localization [3] as well as instability of the calibration [1]. The testing component may also involve full-field optical measurement [2,3,4,5,6,7,8].

A common and simple approach for identifying material parameters is to use the tensile test in which a coupon is subjected to a force while being measured for deformation. Both are global quantities. To extract the material properties, the coupon, usually of simple geometry, can be modeled using the Finite Element Method which incorporates the material model to be calibrated.

The methodology for conducting a calibration requires the construction of a distance functional to quantify the distance between the experimental and computational results:

$$f(x) = \sum_{j=1}^n [\varphi_j(x) - \tilde{\varphi}_j]^2 \quad (1)$$

where  $\varphi_j(x)$  are the components of a force history or force-displacement vector and  $n$  is the number of observation states. The vector  $x$  represents the unknown material parameters and the  $\sim$  represents the experimental results. Further investigation is required to find a method suitable for interpolating values  $\varphi_j$  which correspond to  $\tilde{\varphi}_j$ . This depends on whether  $\varphi$  represents a *mathematical function* (each input has exactly one output), or not. Functions can typically be handled with a least squares functional in which the interpolation of the computed curve is ordinate-based. For non-functions, such as when loading-unloading occurs, more sophisticated techniques are available such as *Partial Curve Mapping* [9,10]. In this method both curves are traced based on preservation of the interval length along the target curve.

While simple material models can typically be uniquely identified using a tensile and/or shear test, a major difficulty in parameter identification is ill-posedness of the observation equation [1]:

$$A(x) = d ; x \in X \quad (2)$$

in which the mapping  $A$  represents the modeling (e.g. a FE model),  $x \in X$  represents the model parameters (the material constants) bounded by the parameter space  $X$  and  $d$  represents the data (experimental data) in the observable data space  $D$ . This problem is typically solved with a minimization problem [1]:

$$d = \arg\{\text{Min}_{d'} J(d'; x)\} \equiv A(x) \quad (3)$$

In Reference [1] Bui lists important issues to check when solving the inverse problem, namely (i) stability of the solution with respect to variations in the data  $d$  as well as with respect to modeling errors and small changes in the model space  $X$  (robustness). It should be mentioned that *the inverse problem to determine the parameters  $x$ , for given experimental data  $d$ , is generally ill-posed*. In material parameter identification, various conditions can cause ill-posedness, for example [1]:

- False experimental data (measurement errors or erroneous data files)

- Incompatible data, i.e. there is no set of material parameters that will cause the model to produce results in data space D.
- Noise in the experimental data
- Modeling errors e.g. in the constitutive model or coarse approximation of the model A

These problems are manifested because of the lack of suitable information provided by the chosen test. E.g. providing global information such as a force-displacement curve representing a chosen point or cross-section of a coupon may not be sufficient to characterize a nonlinear material model which involves material flow, failure and/or damage. It is also typical of failure behavior to be localized, which eludes capture by global force-displacement data [3]. It is probably safe to assume that the more sophisticated the material model and the phenomena it is intended to model, the more parameters it possesses and the greater the need exists for full-field calibration to capture localization.

While the regression problem can always be solved, the deficiency in the distribution of the input data may result in instability of the solution. It is with this problem, as well as accuracy, in mind that experimental mechanicians, over the last three decades, have introduced full field optical measurement techniques. These allow more complete sampling in order to capture phenomena to which the material parameters have non-zero sensitivity, thereby improving stability of the calibration.

The purpose of these non-contact methods is to measure the spatial distribution of physical quantities such as displacement or strain. Much of the development in this area arose from the improvements made to camera and computer technology as well as analysis techniques such as the Finite Element Method. Improvements in optimization methods and techniques have undoubtedly also led to greater sophistication and accuracy in characterizing material properties, but are not able to surmount inherent deficiencies such as noise or bias error. Multiple optical measurement methods have been developed such as photoelasticity (a technique invented in the early part of the twentieth century), digital holography, speckle interferometry, magnetic resonance imaging (MRI) see e.g. [7] and the method used in this paper: Digital Image Correlation.



*Fig.1: Tensile testing equipment and optical measurement system by GOM ARAMIS.*

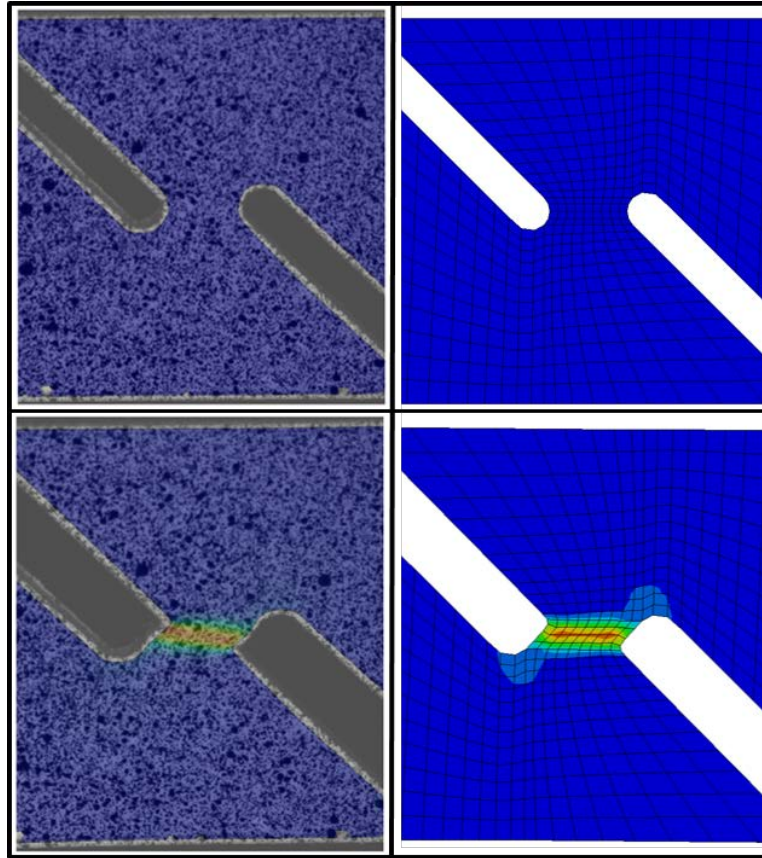


Fig.2: Full field measurement of a shear test using Digital Image Correlation. On the left is the DIC image (GOM ARAMIS) while a strain contour plot is featured on the right (LS-PrePost®).

Digital Image Correlation (DIC) (see e.g. [8]) appeared in the early 1980s and is an optical measurement method (see Fig. 1 for test setup) which provides full-field displacement measurements for mechanical tests of materials and structures. A specific advantage of this tool is that it exploits numerical images acquired at difference stages of loading. As such, it can be used to obtain temporal displacement, deformation or strain fields from an experimental coupon and can be combined with Finite Element Analysis to identify the constitutive properties of a material (see Fig. 2).

Using DIC results, optimization is used to obtain the parameters which will minimize the distance functional involving the measured field and the computed field as components. As expressed for instance in Mahnken et al [3] the functional used is:

$$f(\mathbf{x}) = \sum_{j=1}^n \|\boldsymbol{\varphi}_j(\mathbf{x}) - \tilde{\boldsymbol{\varphi}}_j\|^2 \quad (4)$$

where  $\boldsymbol{\varphi}_j(\mathbf{x})$  is a vector of nodal displacements or strains at a number of observation points and  $n$  is the number of observation states. The functional can be augmented to incorporate global force-displacement measurements or any other functional resulting in parameter identification based on a multi-scale DIC (see e.g. [5]).

## 2 Methodology and software features

While LS-OPT has included parameter identification features since its first commercial release in 2000, the current development goal is to significantly enhance these capabilities to enable LS-OPT to accommodate modern testing techniques such as DIC. While full field calibration has been conducted using LS-OPT in the past [7], the current implementation generalizes the feature to enable it to address a greater diversity of problems.

A summary of essential features, most of which have now been implemented in LS-OPT, follows:

1. A central feature of the methodology is the multi-point history, a basic mathematical entity representing both spatial and temporal dimensions.
2. To access test data, an interface to the GOM ARAMIS DIC software was developed.
3. An algorithm was developed to map a test point cloud to an FE model.
4. The ability to interpolate fields within a finite element is incorporated into the mapping approach.
5. MSE distance functionals for multi-point histories can be used as objective functions.
6. Error analysis enables the user to assess the size of the mismatch as well as the resulting uncertainty of the parameters.
7. Graphical features are available to enhance the prior inspection and editing of test results.
8. Distance contour maps are provided for post-processing the discrepancy between computed values and experimental quantities.
9. Confidence intervals of the material parameters enable the user to quantify their uncertainty.
10. The DynaStats feature of LS-OPT provides sensitivity analysis and stochastic influence tools to identify spatial strain or displacement sensitivities to individual material parameters.
11. The 'overlap' fraction between experimental and computational results. In ordinate-based interpolation methods not all test points may be assignable to a corresponding computed value. The overlap is defined as  $\alpha = m_{\text{interp}}/m_{\text{total}}$  where  $m_{\text{interp}}$  is the number of test points which interpolate to corresponding computed values and  $m_{\text{total}}$  is the total number of test points  $\times$  total number of time states. A poor overlap diminishes the ability to accomplish accurate matching and may induce instability.

A more detailed discussion is provided in the following sub-sections.

## 2.1 GOM ARAMIS interface and alignment of DIC points

Since the test example which follows uses the GOM ARAMIS measurement software, an LS-OPT GOM interface was implemented to define input files, result components and alignment data. The alignment is computed using the least squares formulation shown in the equation:

$$\min_{\mathbf{T}} \|\mathbf{X}_{\text{Test}}\mathbf{T} - \mathbf{X}_{\text{FE}}\| \quad (5)$$

to match any number of test points  $\mathbf{X}_{\text{Test}}$  to corresponding coordinates on the FE mesh  $\mathbf{X}_{\text{FE}}$ . The points in  $\mathbf{X}_{\text{Test}}$  and  $\mathbf{X}_{\text{FE}}$  respectively do not have to correspond exactly as the alignment is based on a least squares principle that will minimize the fitting error for any number of points. The solution of Eq. (5) yields the transformation matrix  $\mathbf{T}$  which is then used to transform all the test points (see e.g. Fig. 7). The data can also be specified as nodal/point IDs. Three or four points normally suffice, but any number can be specified. Alternatively, the alignment step can be omitted, since post-processing software (LS-PrePost<sup>®</sup>) can be used to pre-align the point set.

To enable the creation of cross-plots from the GOM data, both the X- and Y-components shown in Fig.3: can be histories or multi-point histories. E.g. a multi-point  $xx$ -strain can be crossed with a multi-point  $yy$ -strain to create multi-point stress-strain cross-plots or, as in the example that follows in the next section (Fig. 11), the full-field  $xx$ -strain can be crossed with the global force history to create multi-point strain-force cross-plots.

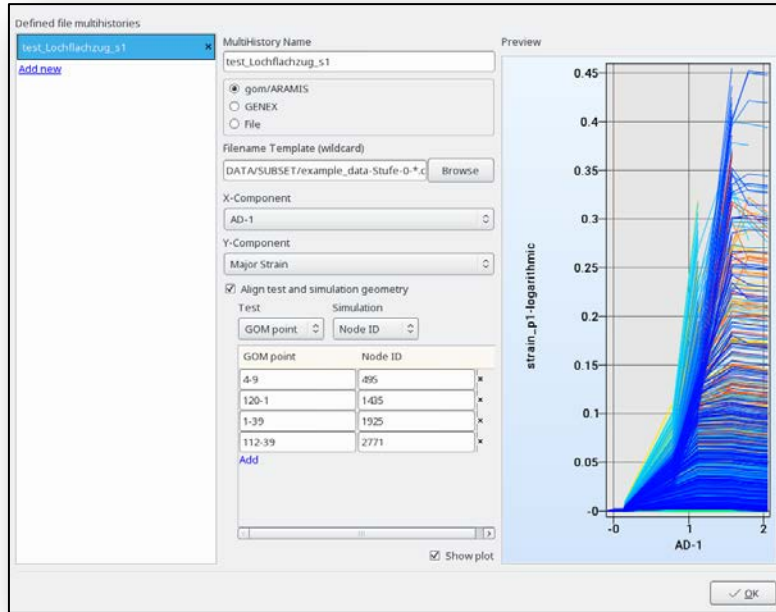


Fig.3: GOM ARAMIS interface in LS-OPT showing alignment input and verification plot of selected test value X- and Y-components.

## 2.2 Multi-point histories

In the GOM ARAMIS option in the multi-point histories interface, each history is computed at a location selected from the test point set in the original, undeformed state. Features are provided to preview the test point alignment (see Fig. 4). Fig. 5 shows three representative deformation states representing 4557 points extracted from the GOM database for a plate with a hole while Fig. 6 shows the FE mesh with corresponding test points. Fig. 7 shows the effect of the least squares point alignment using Eq. (5).

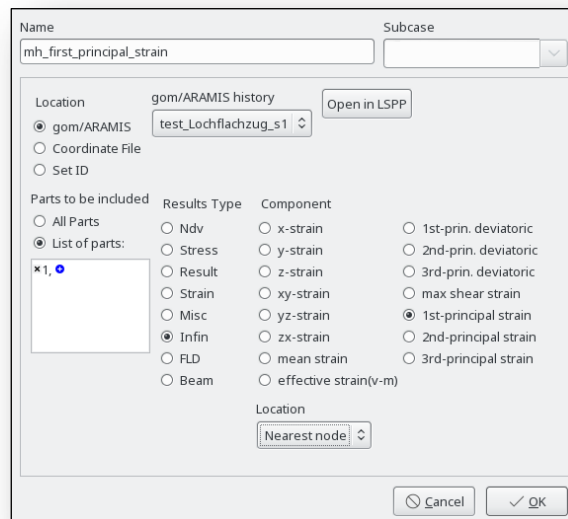


Fig.4: Multi-point history interface enabling the definition of the response type and location data. Location type can be defined as 'nearest node' or 'element'. In the latter option, the result is interpolated at the precise location within the nearest element.

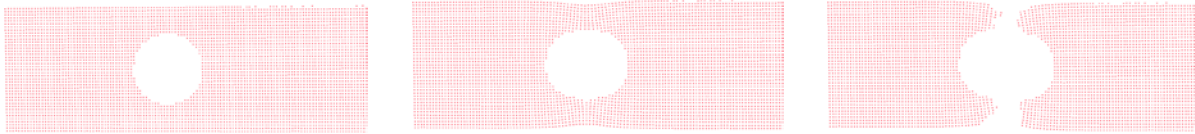


Fig.5: Selected deformation states from GOM output.

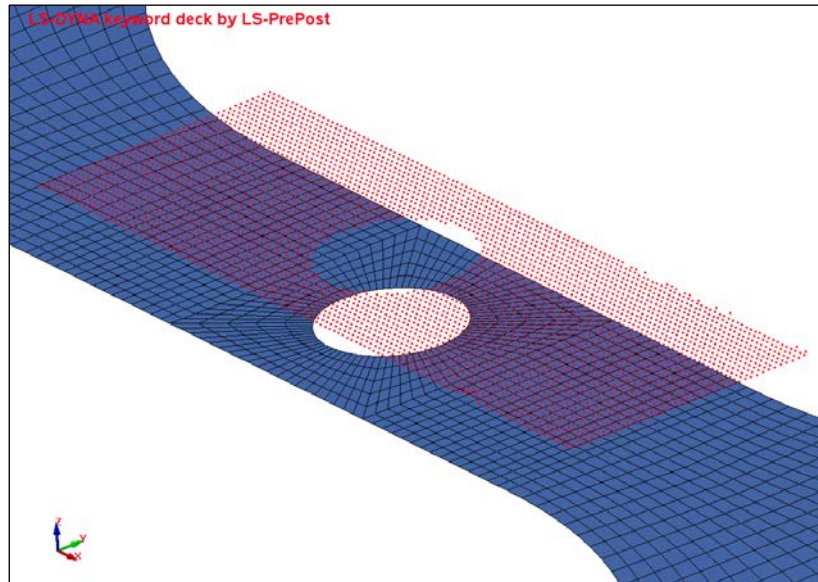


Fig.6: Example of test point mapping showing test point set (red) of 4557 points in relation to the Finite Element mesh.

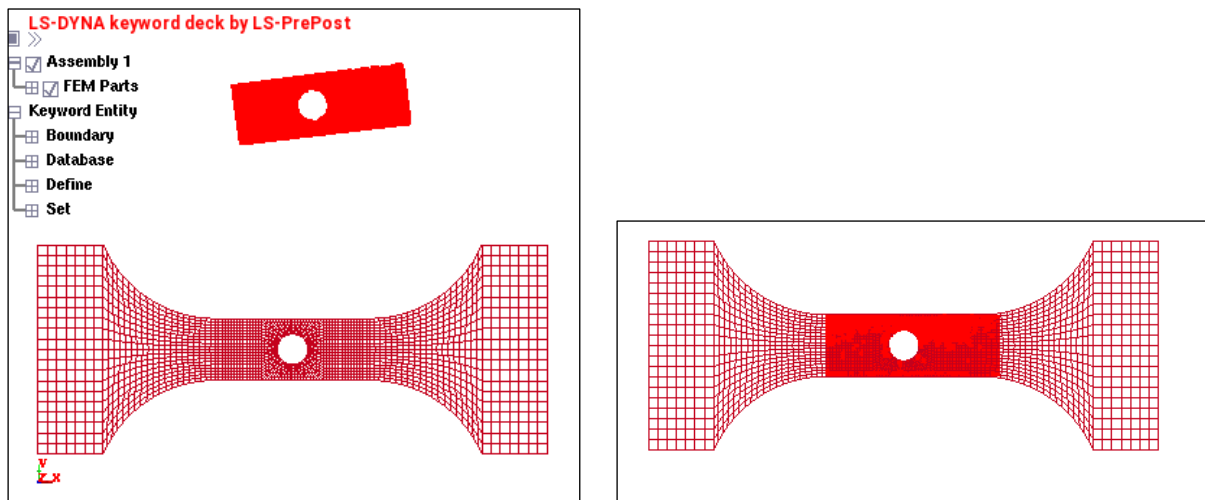


Fig.7: Interactive feature for verification of least squares test point alignment. The starting test point location (in bright red) is shown on the left.

### 2.3 Mapping of test points to a FE mesh

After alignment, the test points are mapped to the FE mesh. The algorithm enables mapping in 3 dimensions using a binary tree algorithm embedded in LS-OPT. The approach allows for an exact nearest neighbor search with the capacity to map  $10^7$  query points to  $10^7$  reference points in

reasonable time (suitable for interactive use). Practical examples encountered thus far have been limited to several thousand points, allowing a practically instantaneous solution. LS-OPT extraction is done in parallel anyway, so time taken for mapping is of little consequence.

The ability to interpolate fields within a finite element is incorporated into the mapping approach. This methodology can interpolate a strain in the nearest element. This is especially important for coarse meshes or high resolution DIC. Obviously, there could still be some discretization error, so the finer the FE mesh, the more accurate the interpolated value will be.

### 3 Example: Tensile test

An example of a tensile test was selected to test and demonstrate the full-field calibration feature in LS-OPT (Figs. 1 and 8). Fig. 9 shows the force-displacement trajectory as well as the strain contours at the time state depicted in the plot. The necking phenomenon is clearly visible from the test images in Fig. 9.

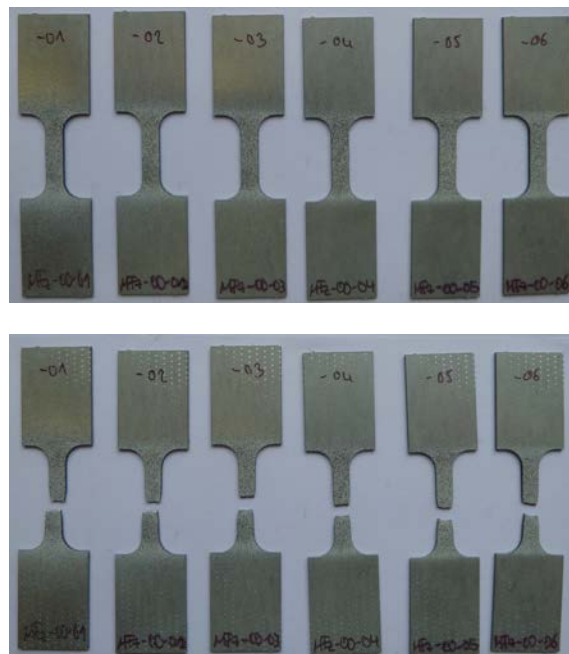


Fig.8: Test coupons for a tensile test (0° w.r.t. rolling direction) (Sample numbers MFz-00-\*)

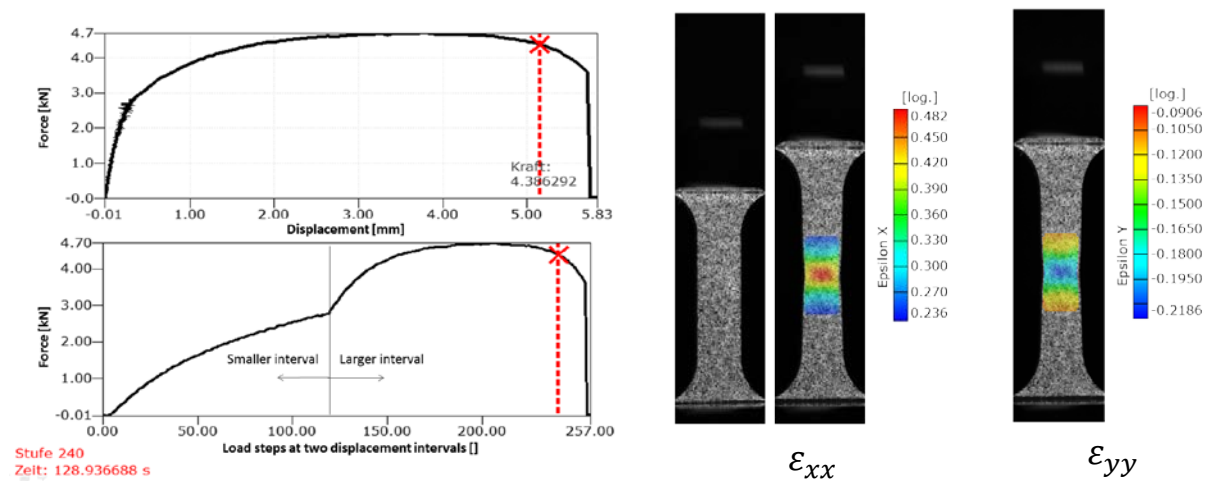


Fig.9: Sample MFz-00-01: Force-displacement diagram and DIC contour plots for  $xx$ - and  $yy$ -strains.

### 3.1 Simulation

A Finite Element model was created in LS-DYNA<sup>®</sup> [11] to model a typical coupon subjected to a tensile force. The material model uses the von Mises yield locus and a Hockett-Sherby flow curve formula for extrapolation beyond the point of a uniform strain state:

$$f(\varepsilon_p) = A - B e^{-C \varepsilon_p^N} \quad (6)$$

where  $A$ ,  $B$ ,  $C$  and  $N$  are material constants.  $C_1$ -continuity is assumed at the flow transition following the uniform strain state which removes the requirement to incorporate  $A$  and  $B$  in the optimization that follows.

### 3.2 Optimization

The LS-OPT setup required alignment of the measured points with the FE mesh as shown in Fig. 10. The force vs. point-wise  $\varepsilon_{xx}$  strain curves are shown in the preview feature depicted in Fig. 11. Each curve represents a measuring point as shown in black in Fig. 10. For the optimization, a cross-plot was defined using multi-point histories to represent the global force vs. point-wise strains.

The optimization problem was set up with parameters  $C$  and  $N$  as variables and with the objective to minimize the distance functional  $f$  [Equation (4)]. This defines the ideal of matching  $\varepsilon_{xx}$  at each point and each deformation state. The optimization was conducted using the Sequential Response Surface method of LS-OPT [10].

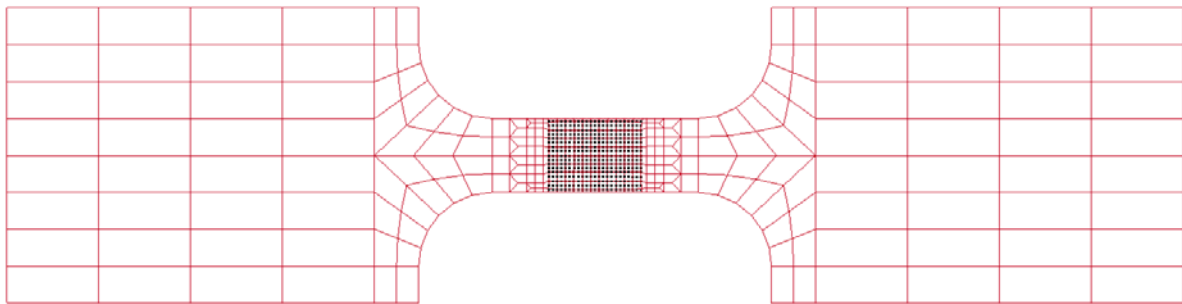


Fig.10: Finite element model of the coupon specimen (red) shown with 391 superimposed optically measured points at the center (black).

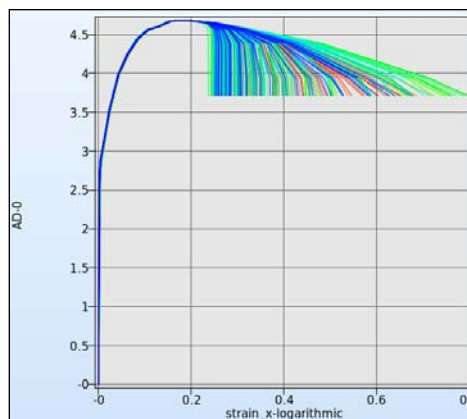


Fig.11: Preview of the multi-point curve: the force vs. full-field logarithmic  $xx$ -strain as rendered in a previewing feature of the GOM interface in LS-OPT. Each curve represents a single measuring point.



#### 4 Results and observations

The optimization history of the distance functional is shown in Fig. 12. The value of the distance functional (the graph ordinate) [Eq.(4)] has been normalized with the maximum absolute value of the measured values. The table in Fig. 13 represents a comparison of the  $xx$  strain contours obtained from the GOM software with the contours obtained from the LS-DYNA FE simulation for a set of initially estimated values of  $N = 5$  and  $C = 1$ . The optimization yields values  $N = 0.194$  and  $C = 0.0556$  which corresponds to the results of Fig. 14. It can be seen that the computational result in the latter figure is significantly closer to the experimental result.

A second optimization run from a different starting point (not shown here) yielded values 0.226 and 0.0717 for  $N$  and  $C$  respectively. Several observations can be made:

1. The optimization result converges to a solution around the 10th iteration.
2. Different starting points may yield different optimal parameters which, while not excessive, cannot be ignored entirely.
3. The objective value varying between 0.0396 (baseline) and 0.0377 (It. 10) is a relatively small variation.

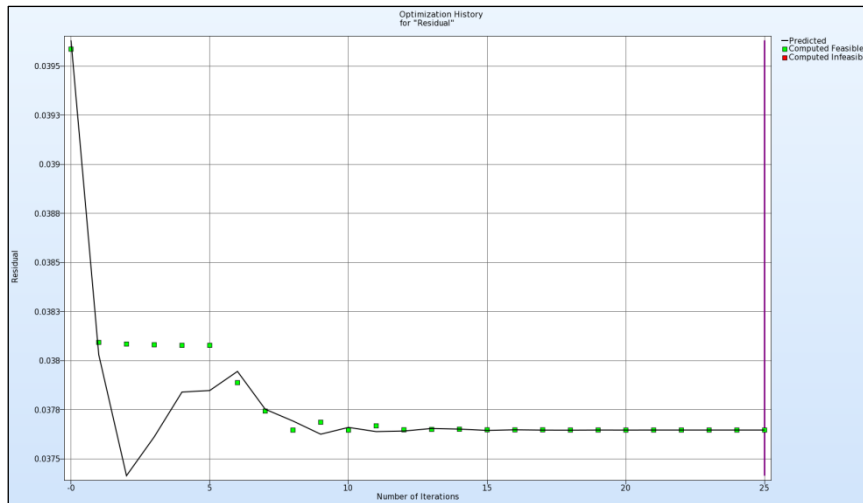


Fig.12: Optimization history of the normalized distance functional showing convergence achieved between 10 and 15 iterations. The points represent LS-DYNA results while the line represents the response surface approximation values.

| Force vs. displacement plot showing deformation state (red dotted line) | $\epsilon_{xx}$ (FE model) | $\epsilon_{xx}$ (GOM ARAMIS test) |  |
|---|----------------------------|-----------------------------------|--|
|   |                            |                                   |  |
|   |                            |                                   |  |

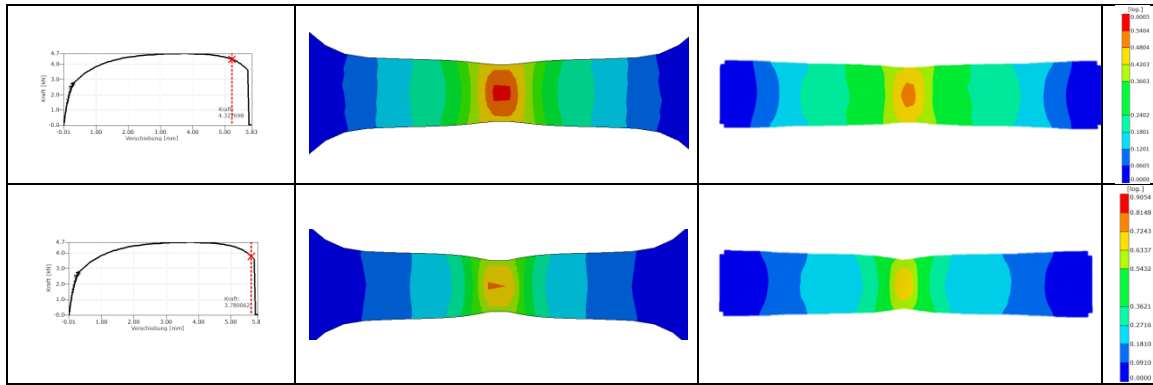


Fig.13: Baseline parameters  $N = 5$  and  $C = 1$ : Computational vs. measured  $\epsilon_{xx}$  strain field contours at various deformation states (contour plots not to scale). The computational and measured values use the same color scale depicted in the right-most column, so can be compared directly.

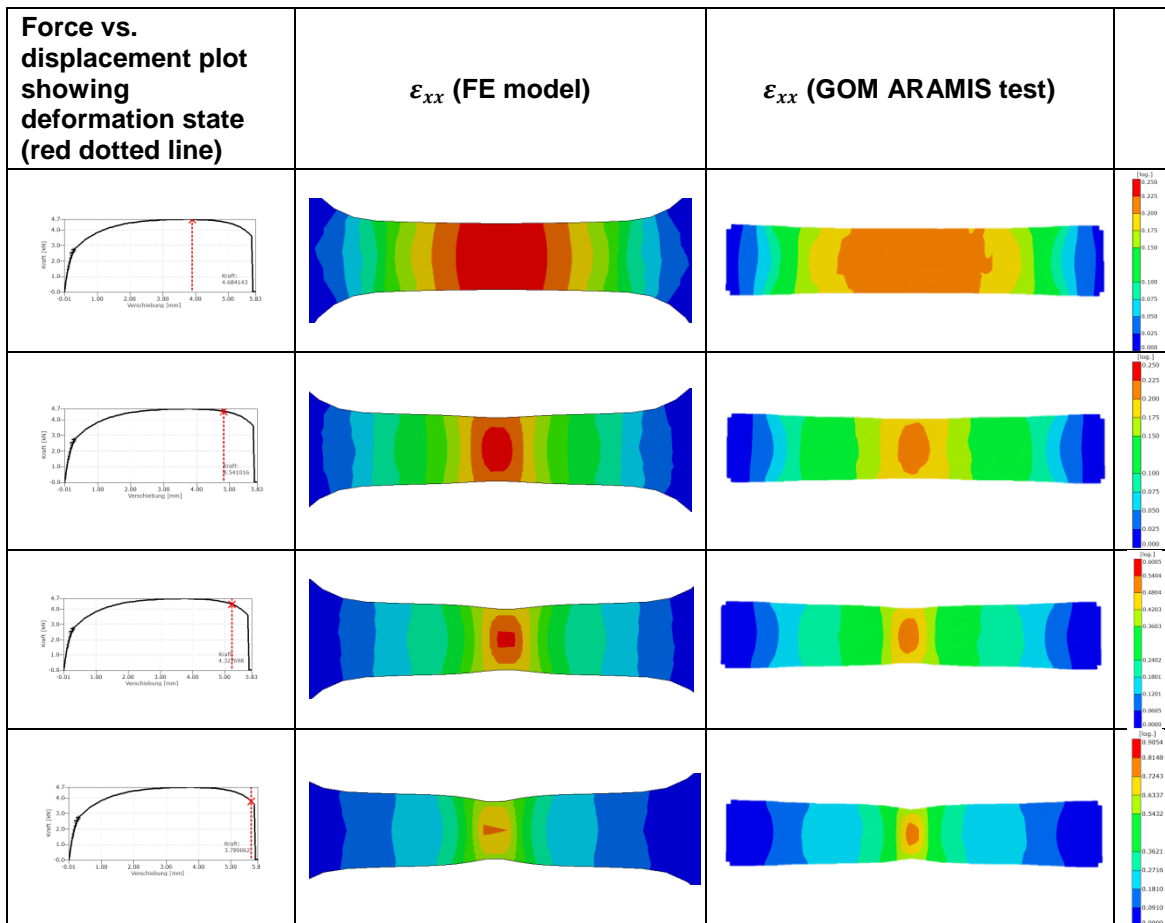


Fig.14: Optimal parameters  $N^* = 0.194$  and  $C^* = 0.0556$ : Comparison of computational vs. measured  $\epsilon_{xx}$  strain field contours at various deformation states (contour plots not to scale). The computational and measured values use the same color scale depicted in the right-most column, so can be compared directly.

## 5 Summary and conclusions

A parameter identification has been executed using the LS-OPT optimization tool incorporating a distance function based on multi-point histories and DIC experimental results obtained from a tensile test using the GOM ARAMIS software.

While the study has validated the code implementation, several deficiencies were observed and are explained below, with a view to address them in future development:

1. **Stability and Uniqueness.** It was shown that different starting points for the optimization procedure yield slightly different results which presumably affect the accuracy of the calibration result. Possible reasons are (i) the inability of the SRSM optimization algorithm to converge sharply, (ii) the presence of local minima (mathematical non-uniqueness) and (iii) instability of the solution. Both the reasons (i) and (ii) can only be addressed by switching to a different optimization algorithm, such as the Genetic Algorithm available in LS-OPT. Point (iii) can only be addressed by investigating the suitability and location of the quantities measured in the formulation of the objective. It should be noted that only  $\varepsilon_{xx}$  was used in the calibration, while  $\varepsilon_{yy}$  was neglected, a factor which may have influenced the stability of the solution. (See also the section on sensitivities below).
2. **Sensitivity.** A methodology that can be used to investigate stability is sensitivity analysis. It is therefore suggested that a study be done, using LS-OPT DynaStats, in which the sensitivity (or stochastic influence) contours are studied to determine locations where sensitivities of response types such as  $\varepsilon_{xx}$  and  $\varepsilon_{yy}$  to the individual material parameters are highest. This could provide a general tool for investigating the suitability of response field types and their corresponding spatial distribution. No further development is required.
3. **Confidence intervals of the parameters.** It is also suggested that confidence intervals be calculated for the parameters, a function which will require the calculation of the gradients (with respect to the parameters) of the multi-point histories at the optimal solution. The confidence intervals signify the degree to which the optimal value of a parameter can be trusted, and may provide a clue as to inadequate experimental data, especially to the user intimately familiar with the material model. Confidence intervals would require the definition of a mathematical composite (currently also used with virtual histories in LS-OPT) based on response surfaces and is presently under development.
4. **Noise.** The very slight improvement of the objective function (0.0396 vs. 0.0377) seems to suggest that a significant component of the residual error (of the distance functional) contains noise so that fitting the material model to the test always yields a non-zero residual. The noise may emanate from discretization error and/or experimental error.
5. **Modeling error.** It is likely that, in addition to noise, the material flow model does not represent the experimental response with absolute accuracy. This causes a bias or modeling error which remains a residual error even after finding a converged solution to the regression problem.
6. **Discretization error.** The FE mesh provided for the example is somewhat coarse, possibly resulting in a discretization error. This may be especially true because triangular elements are used in the transitions. A remedy would be to increase the fineness of the mesh and to use only higher order triangles or quadrilateral elements.
7. **Curve matching technique.** It is apparent from Fig. 11 that some of the curves have very steep post-yield behavior which presents a difficulty for ordinate-based interpolation. As a consequence some of this curve data may be inadvertently amiss. A possible solution would be to extend the *Partial Curve Mapping* capability in LS-OPT (see [9,10]), currently available for simple histories, to multi-point curves.

## 6 References

- [1] Bui, H.D. *Inverse Problems in the Mechanics of Materials, An Introduction* (CRC Press, Boca Raton, London) (1994).
- [2] Pagnacco, E., Moreau, A., Lemosse, D. Inverse Strategies for the identification of elastic and viscoelastic material properties using full-field measurements, *Materials Science and Engineering*, Vol. 452-453, pp. 737-745, 2007
- [3] Mahnken, R., Stein, E. Parameter Identification for Finite Deformation Elasto-Plasticity in Principal Directions, *Comput. Methods Appl. Mech. Engrg*, 147, 17-39 (1997).

- [4] Leclerc, H., Périé, J.-N., Roux, S., Hild, F. Integrated Digital Image Correlation for the Identification of Mechanical Properties, *MIRAGE 2009, LNCS 5496*, pp. 161-171, 2009, A Gagalowicz and W. Philips (Eds.), Springer-Verlag 2009.
- [5] Passieux, J.C., Bugarin, F., David, C., Périé, J.-N., Robert, L. Multiscale Displacement Field Measurement Using Digital Image Correlation: Application to the Identification of Elastic properties, <https://hal.archives-ouvertes.fr/hal-00949038> (2014).
- [6] Gu, J., Cooreman, S., Smits, A., Bossuyt, S., Sol, H., Lecompte, D. and Vantomme, J. Full-field optical measurement for material parameter identification with inverse methods, *High Performance Structures and Materials III, WIT Transactions on the Built Environment*, Vol. 85, 2006. doi10.2495/HPSM06024.
- [7] Stander, N. The identification of myocardial material parameters from spatial tagged MRI strain data using LS-OPT and LS-DYNA, Report, LSTC In cooperation with J. Guccione, Cardiac Mechanics Lab, UCSF. (2006).
- [8] *Full Field Measurements and Identification in Solid Mechanics*, Eds. Grédiac, M., Hild, F., Wiley 2013.
- [9] Witowski, K., Stander, N. Parameter Identification of Hysteretic Models Using Partial Curve Mapping, *Proceedings of the 12<sup>th</sup> AIAA Aviation Technology Integration and Operations Conference and 14<sup>th</sup> AIAA/ISSMO Multidisciplinary Analysis and Optimization Conference*, Indianapolis, Indiana, 2012.
- [10] Stander, N., Roux, W.J., Basudhar, A., Eggleston, T, Craig, K.-J. *LS-OPT Users Manual, Version 5.2. December 2015.*
- [11] Hallquist, J.O. *LS-DYNA Users Manual, Livermore Software Technology Corporation.*